Maximum Entropy Spectral Reconstruction of Nonuniformly Sampled Data

MEHDI MOBLI,[1] JEFFREY C. HOCH[2]

[1] *Institue for Molecular Bioscience, The University of Queensland, St. Lucia, QLD 4072, Australia*
[2] *Department of Molecular, Microbial, and Structural Biology, University of Connecticut Health Center, Farmington, CT 06030-3305*

ABSTRACT: The time required to complete a multidimensional NMR experiment is directly proportional to the number of evolution times sampled in the indirect dimensions. A consequence when utilizing conventional methods of data acquisition and spectrum analysis is that resolution in the indirect dimensions is frequently sample-limited. The problem becomes more acute at very high magnetic fields, where increased chemical shift dispersion requires shorter time increments to avoid aliasing. It has long been recognized that a way to avoid this limitation is to utilize methods of spectrum analysis that do not require data to be sampled at uniform intervals, permitting the collection of data at long evolution times requisite for high resolution without requiring collection of data at all intervening multiples of the sampling interval. Several promising methods have evolved that are seemingly quite different, yet can be shown to yield similar results when applied to similar sampling strategies, emphasizing the importance of the choice of samples, regardless of the technique used to compute the spectrum. Maximum entropy (MaxEnt) reconstruction is a very general method for spectrum analysis of nonuniformly sampled data (NUS), and because it can be used with essentially arbitrary sampling strategies and makes no assumptions about the nature of the signal, it provides a convenient basis for exploring the influence of the choice of samples on spectral quality. In this article we use this versatility of MaxEnt reconstruction to compare different approaches to NUS in multidimensional NMR and suggest strategies for improving spectral quality by careful choice of sample times. Concepts Magn Reson Part A 32A: 436–448, 2008.

KEY WORDS: NMR; signal processing; nonuniform sampling; nonlinear sampling; sparse sampling; sampling artifacts; maximum entropy; projection reconstruction

Received 25 July 2008; revised 26 September 2008; accepted 13 October 2008

Correspondence to: Jeffrey C. Hoch; E-mail: hoch@uchc.edu

Concepts in Magnetic Resonance Part A, Vol. 32A(6) 436–448 (2008)
Published online in Wiley InterScience (www.interscience.wiley.com). DOI 10.1002/cmr.a.20126

INTRODUCTION

Applications of NMR spectroscopy continue to expand as high field magnets and cryogenic probes attain ever higher levels of sensitivity and resolution (*1*). Yet for many applications, the additional resolution afforded by resolving resonances along multiple dimensions remains essential. This is especially important for biomolecular NMR, where there is a growing need to investigate larger and more complex molecules and molecular assemblies. Along any dimension the frequency resolution is closely related to the length of the time domain data record. Because the time required to complete a multidimensional experiment is directly proportional to the number of samples collected in the indirect dimensions, obtaining high resolution in the indirect dimensions can require impractically long experiments. The problem becomes more acute at high magnetic fields, where increased spectral dispersion necessitates shorter intervals between samples and thus more samples to achieve long evolution times.

It has been recognized for some time that a key factor limiting resolution along the indirect dimensions of multidimensional experiments is the requirement that samples be collected at uniform intervals, a requirement imposed by the discrete Fourier transform (DFT) and methods such as linear prediction (LP) extrapolation (*2*). Recently several different approaches to overcome this obstacle have been developed. Although they use different methods to compute the multidimensional spectrum from time domain data, they all relax the requirement that samples be collected at uniform intervals (*3–16*). We refer to this general approach as nonuniform sampling (NUS). NUS enables collection of data at long evolution times, and thus affords high frequency resolution without imposing the time consuming burden of collecting long data records.

While the different methods used to obtain the spectrum from NUS data exploit fundamentally different mathematics, it has recently been shown that the features of the reconstructed spectrum are predominantly influenced by the NUS strategy employed and not by the specific processing technique (*17*, *18*). This suggests that insights into the design of efficient NUS strategies obtained using one processing method should in principle be applicable to the other approaches. Here we have chosen to use maximum entropy (MaxEnt) spectral reconstruction as the means for computing multidimensional spectra from NUS data, but our emphasis will be on the influence of different NUS strategies on the spectra. Although experimental noise constitutes a fundamental limiting factor confronting all methods of spectrum analysis in NMR, our focus here is on the sampling artifacts, or sampling noise, that is invariably introduced by NUS. Before introducing various NUS strategies and MaxEnt, however, we briefly review the fundamentals of uniform sampling.

UNIFORM SAMPLING

In the seminal development of pulsed Fourier transform NMR by Ernst and Anderson (*19*), the response of a nuclear spin system to an RF pulse is the free induction decay (FID). Sampled at uniform time intervals, DFT yields the frequency spectrum. The Nyquist sampling theorem states that a wave must be sampled at least twice per cycle in order to be completely characterized (*20*). The sampling interval or dwell time Δt determines the highest frequency that can be unambiguously determined (*21*). This frequency range is referred to as the spectral width SW and for single-phase detection is equal to one-half the reciprocal of the dwell time; for quadrature phase detection, in which components 90° out-of-phase with respect to each other are sampled simultaneously, SW is the reciprocal of the dwell time. A signal with a frequency higher than SW will appear in the DFT spectrum at an incorrect frequency. This phenomenon, called aliasing or folding, will be familiar to any viewer of old western movies in which wagon wheels appear to reverse direction as they are slowing down (*21*). This is demonstrated in Fig. 1 where a signal with a frequency inside the spectral window can not be distinguished from a signal with a frequency shifted higher by an amount equal to SW. The location of aliased frequencies depends on an additional detail of the sampling, namely whether and how phase-sensitive data acquisition is employed (*22*).

Another important aspect of sampling is the length of time that a signal is sampled. The longer a signal is allowed to evolve, the easier it is to resolve components with similar frequencies. This is illustrated in Fig. 2, where it is apparent that two sinusoids with similar frequencies are more readily distinguished at long evolution times. A complicating factor is that when sampling data containing decaying signals, at long evolution times the contribution of noise will eventually swamp the contribution from the signals. At this point no further information about the signals can be extracted. The signal-to-noise ratio (S/N) of an experiment thus determines how many sample points can be acquired before the signal

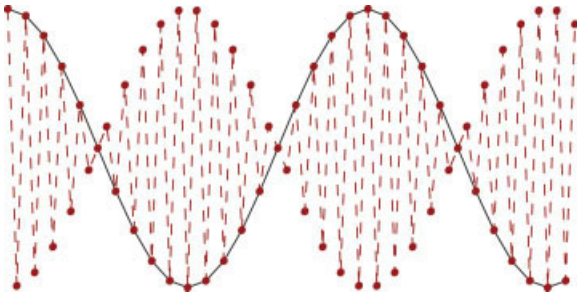

Figure 1 A sinusoid with frequency ω (dotted line) will appear to have a lower (aliased) frequency (bold line) when sampled at an interval corresponding to a spectral width smaller than ω. Here the dotted sinusoid is sampled at an interval corresponding to SW = F > ω. Using every other sample results in SW = F/2 < ω. [Color figure can be viewed in the online issue, which is available at www.interscience.wiley.com.]

begins to vanish below the noise. It has been shown that the point of diminishing returns where collecting additional data samples begins to degrade S/N in the spectrum is $1.5T_2^*$ (*3*, *23*). The need to avoid aliasing while acquiring data at long evolution times imposes a dual constraint on data collection; on the one hand closely spaced sample points are required to avoid aliasing and on the other hand samples at long evolution times are required to distinguish similar frequencies.

For multidimensional experiments in which S/N is sufficiently high to preclude signal averaging, the principal determinant of the time required to perform an experiment is the number of samples collected along the indirect dimensions, sometimes referred to as the "sampling limited" regime (*24*). There are two broad classes of approaches for reducing the time cost of obtaining high resolution in the indirect dimensions. One class employs methods capable of obtaining high-resolution spectra from short, uniformly sampled data records, such as linear prediction (LP) extrapolation and the filter diagonalization method (*19*). The other class, the focus of this work, employs NUS.

Several different strategies for NUS have been applied in NMR. In a seminal work, Barna et al. introduced the concept of random sampling biased to match the exponential decay of the signal envelope (*26*). More recently, reduced dimensionality (RD) (*12*, *27*), back-projection reconstruction (BPR also known as PR) (*28*), G-transform Fourier transform (GFT) (*11*), and projection decomposition (*5*) methods have been introduced which share a common strategy for NUS that involves coupled evolution times. This results in sampling along radial vectors in time. While NUS approaches based on radial sampling typically utilize methods for computing the frequency spectrum that are restricted to this special sampling strategy (e.g. BPR and GFT), in general it is possible to dissociate the strategy used to implement NUS from the method used to compute the spectrum from NUS data. Methods of spectrum analysis that are applicable to essentially arbitrary NUS strategies include Bayesian (*29*), maximum likelihood (MLM) (*14*), MaxEnt reconstruction (*25*, *30*), forward maximum entropy method (*31*), iterative thresholding or minimum l_1-norm reconstruction (*32*), nonuniform DFT (*16*), and multidimensional decomposition (*13*). It has been demonstrated that spectra obtained from NUS data depend mainly on the NUS strategy employed, and to a much lesser extent on the method used to compute the spectrum (*17*). Thus insights gained into the influence of NUS strategies on spectral quality derived using one method will be broadly applicable to other methods of spectrum analysis. In this work we employ MaxEnt reconstruction, because it is more general than the other approaches inasmuch as it makes no assumptions about the signals (and thus it is applicable to experiments giving rise to arbitrary lineshapes), is applicable to experiments of arbitrary dimension (including one- and two-dimensional), and very efficient algorithms exist (*21*, *33*).

NUS AND SAMPLING ARTIFACTS

Any NUS scheme introduces spectral artifacts as a direct result of the excluded data. Such "sampling artifacts" are the major drawback of using NUS methods. While all methods of spectral analysis, with the exception of nuDFT, to some extent attempt to

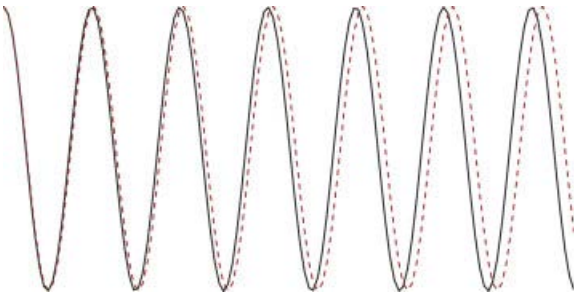

Figure 2 The ability to distinguish two sinusoids with similar frequencies depends on the longest evolution time. [Color figure can be viewed in the online issue, which is available at www.interscience.wiley.com.]

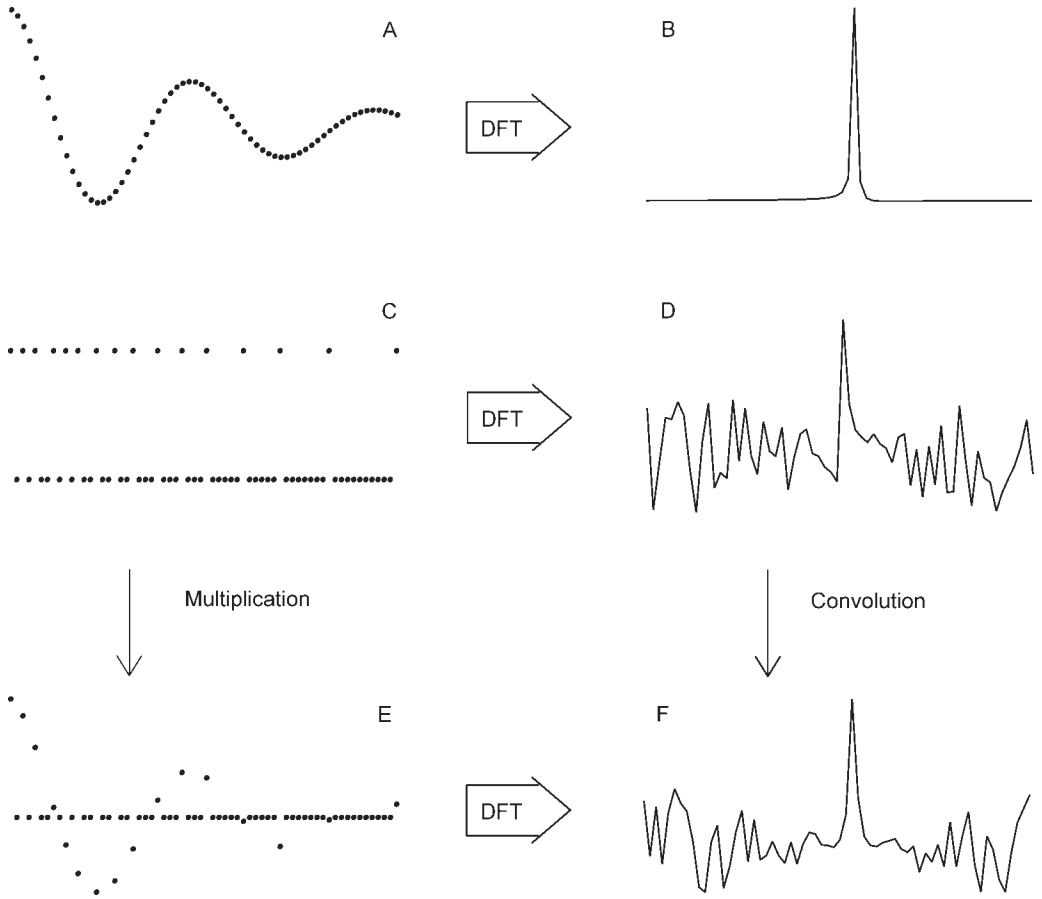

Figure 3 The DFT of a decaying sinusoid (A, B) and a sampling schedule (C, D) and their multiplication in the time domain (E) resulting in their convolution in the frequency domain (F).

mitigate sampling artifacts, minimizing these artifacts can be achieved by proper design of the sampling scheme. To design such schemes it helps to have a basic understanding of the artifacts. The convolution theorem (*34*), which holds that the spectrum of a time series obtained from point-by-point multiplication of two separate times series is equivalent to the convolved spectra of the individual time series enables an insightful analogy.

Consider a one-dimensional FID sampled at N regular intervals according to the Nyquist criterion. We define a NUS sampling scheme to be a subset of $M < N$ samples. Since each of the M samples falls at one of the time intervals characteristic of uniform Nyquist sampling, we refer to this approach as on-grid NUS (we will show later that any off-grid sampling scheme can be reasonably approximated by an on-grid scheme). Now consider a discrete sampling function defined on the Nyquist grid that has the value 1 for each sample that is in the NUS subset and zero for samples not in the set. The problem of recovering the spectrum from NUS data can then be considered as the problem of deconvolving the spectrum of the sampling function, which is called the point spread function (PSF), from the true spectrum of the signal. This follows from the convolution theorem, and is illustrated in Fig. 3. When the signal contains a single frequency component, as shown in the example, it is easy to predict where the sampling artifacts will appear and their relative intensities by examining the PSF; they will appear at the same frequencies relative to the one frequency component as peaks in the PSF are relative to the zero-frequency component of the PSF. When the signal contains more than one frequency component, the sampling artifacts around one frequency component can interfere, constructively or destructively, with sampling artifacts from other frequency components, or with other frequency components themselves.

The example shown in Fig. 3 uses the DFT to compute the spectrum. The application of the DFT to on-grid NUS data where the evolution times not sampled are set to zero is an application of nuDFT.

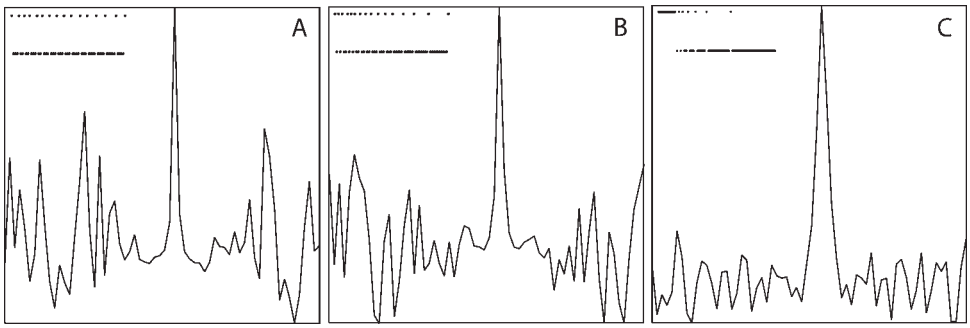

Figure 4 nuDFT of a noiseless, synthetic decaying sinusoid using three different sampling schedules (see also Fig. 3). The sampling schedule is shown in the top left of the panels, where the upper row indicates sampled data points and the lower row indicates those that were not sampled. The decay rate of the sampling schedule increases from A to C, yielding a decrease in sampling artifacts and an increase in linewidth.

Using more advanced methods that attempt to deconvolve the PSF from the spectrum the sampling artifacts can be dramatically reduced, but as we shall see their locations and amplitudes relative to each other are usually preserved.

Based on the analogy with convolution, a sampling schedule that gives rise to a PSF containing weaker nonzero frequency components will give rise to smaller sampling artifacts. A simple way to achieve smaller sampling artifacts is to collect more samples. This comes at the expense of increased experiment time, of course. For a given NUS set size, different arrangements of the sample times result in different PSFs, and thus different sampling artifacts. Faster decay of the sampling density (collecting more data at short times) will yield stronger but broader signals. Conversely, slower decay will yield noisier spectra but sharper lines (Fig. 4). The distribution of the sample points in time governs the manifestation of these artifacts in the spectrum.

The interference of sampling artifacts results from nonorthogonality of the complex exponentials over a set of nonuniformly spaced times. The discrete Fourier transform is an expansion in a set of basis functions consisting of the complex exponentials $e^{-2\pi ikn/N}$ (*21*). The complex exponentials have the important property of orthogonality,

$$\sum_{n=0}^{N-1} e^{2\pi i(k-k')n/N} = 0, \quad k \neq k' \qquad [1]$$

which means that when data is sampled uniformly the complex exponentials with frequencies $2\pi k$ and $2\pi k'$ are independent of one another. For NUS, however, some of the terms in the sum of Eq. [1] are left out (or equivalently, set to zero), and the complex exponentials are no longer orthogonal. Thus one way to view NUS sampling artifacts is that frequencies in the spectrum are no longer fully independent of one another.

Characteristics of Sampling Artifacts

The previous section showed the distribution of sampling artifacts for a zero frequency signal. In the general case of a complex but band-limited signal, each peak will produce a set of artifacts that have the same relative frequencies as peaks in the PSF of the sampling schedule. Thus in principle the positions of the sampling artifacts can be determined if all "true" signals are known a priori. While the relative frequencies and relative amplitudes of the artifacts can be estimated from the PSF, their absolute amplitudes also depend on the intensity of the signal components. They are further in direct proportion to the signal intensity and the extent of interference from sampling artifacts arising from other signal components (Fig. 5). For linear methods of spectrum analysis, the artifacts, like the signals, are strictly additive. For nonlinear methods, such as MaxEnt, sampling artifacts and signals will be subject to the same nonlinearities.

An example illustrating the interference that results from NUS is shown in Fig. 6. Here the variation in peak amplitude in nuDFT spectra computed from NUS time domain data when one of the peak frequencies is varied while the other peak is fixed is apparent. One way of shifting some of the sampling artifacts to extreme values is to select a NUS set from an oversampled grid (with a grid spacing shorter than required by the Nyqusit theorem), or by sampling at completely random intervals (i.e. not restricted to a uniform grid defined by multiples of a fixed dwell time). The former is illustrated in Fig. 7. Note that the Nyquist theorem does not hold for NUS

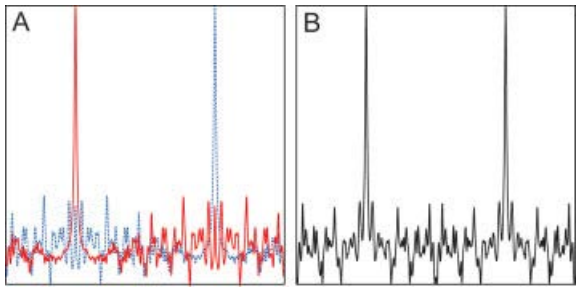

Figure 5 Sampling artifacts, like signals, are additive. Panel A shows the overlay of two different nuDFT spectra, each containing a single frequency component. Panel B shows the nuDFT of the sum of the two NUS data sets. [Color figure can be viewed in the online issue, which is available at www.interscience.wiley.com.]

data, and the phenomenon of aliasing is more complex; for example it is frequency-dependent, and the amplitudes of aliased peaks need not match the amplitude of the true signal.

Dynamic Range

Since the amplitudes of sampling artifacts are a proportional to the amplitudes of the associated signal peaks, it follows that a signal containing components with widely varying amplitudes, or a high dynamic range, will present special challenges to NUS. The sampling artifacts due to one peak may introduce ambiguities in the spectrum that exceed the magnitude of weaker peaks in the spectrum (Fig. 8). For linear methods of spectrum analysis methods such as nuDFT, one can determine a priori the limiting dynamic range for which artifacts arising from a given NUS scheme will obscure weak peaks by comparing the magnitude of the largest nonzero peak in the PSF relative to the magnitude of the zero-frequency component; the ratio gives the limiting dynamic range. For methods that attempt to deconvolve PSF from the spectrum (*35*), more subtle tests must be applied.

MaxEnt and NUS

In the examples presented thus far we have utilized nuDFT to compute spectra for NUS data. While nuDFT serves as a convenient pedagogical tool for understanding the origin and nature of NUS artifacts, there are several other methods that are better suited to NUS because they effectively attempt to deconvolve the NUS PSF from the spectrum. An especially versatile approach that we will employ here is MaxEnt reconstruction. The theory and general properties of MaxEnt reconstruction have been reviewed in detail (*36*).

Derived using information-theoretic principles, MaxEnt reconstruction is often described as yielding the spectrum containing the least amount of information consistent with the measured data. We take a somewhat more pragmatic view in describing MaxEnt reconstruction as a method that uses entropy as a regularizer to yield smooth spectra that are consistent with the measured data. Empirically and theoretically it can be shown that this smoothing is nonlinear: peaks in the MaxEnt spectrum are scaled down, but smaller peaks are scaled down more than larger peaks (*30*). A consequence of this property is that MaxEnt reconstruction is more likely to result in false negatives (missing peaks) than false positives. Our understanding of the nature of the nonlinearities in MaxEnt spectra stands in contrast to the relatively poorly understood nonlinearities associated with other methods of spectral analysis for NUS data. This understanding has enabled techniques for minimizing nonlinearity [such as FM (*31*)] and for compensating for its effects (*30*). In applications where linearity

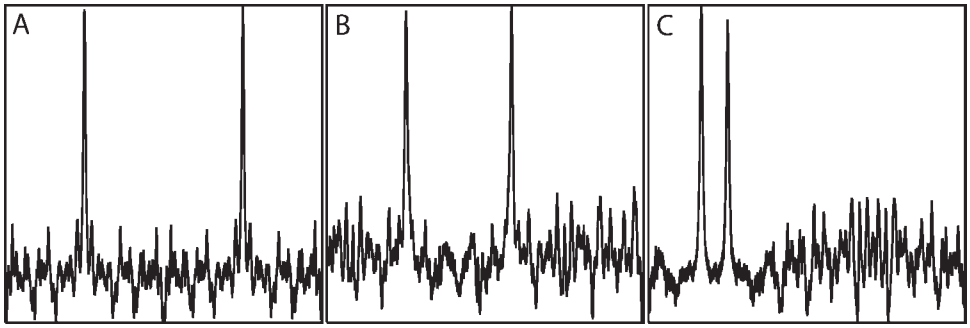

Figure 6 nuDFT spectra of two sinusoids where the frequency of one is held fixed and the other progressively shifts (panel A to C), showing that both the amplitudes of the artifacts and the peaks are modulated by the shifting peak.

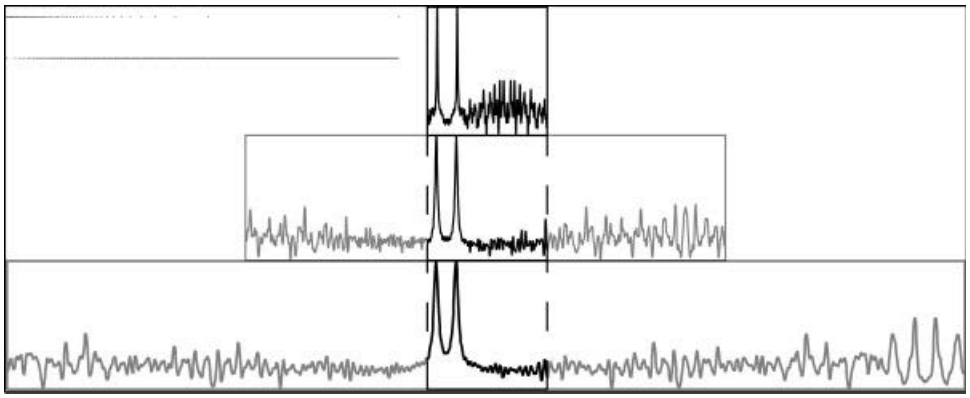

Figure 7 Effect of oversampling. The top panel shows the two peaks and their associated sampling artifacts and the middle and lower panels show the same peaks using 4X and 8X SW. The sampling artifacts are shifted to extreme frequencies at the cost of line broadening.

is required, it is important to take appropriate steps to minimize the nonlinearity or compensate for it (*30*, *37*).

The improvements that can be achieved with MaxEnt are demonstrated in Fig. 9. While the sampling artifacts are greatly reduced compared to the nuDFT spectrum, they are still present in the locations predicted by convolution of the NUS PSF with the true spectrum. The smoothing effect of MaxEnt on NUS artifacts is not merely cosmetic, however, as it diminishes sampling artifacts without suppressing real peaks. This is demonstrated in Fig. 10, where constructive interference from the sampling artifacts of four strong peaks obscure a fifth weaker peak in the nuDFT spectrum, whereas the MaxEnt spectrum efficiently reduces the artifacts without suppressing the real peak.

The ability of MaxEnt to eliminate NUS artifacts is ultimately limited by the presence of noise (which is absent in these examples). For very low noise levels and data with low dynamic range it may be possible to make them effectively vanish by tuning the parameters controlling MaxEnt reconstruction. Rarely are these conditions met in practice, however, and completely noise-free and flat baselines are then usually a sign of over-regularization (*38*).

nD NUS

One-dimensional NUS illustrates some of the general properties of NUS, but the 1D case (i.e. NUS in the indirect dimension of a 2D) has attributes that render it less attractive than multidimensional NUS. One is that NUS artifacts, when applied to a single dimension, exhibit column-wise coherence in which sampling artifacts in adjacent columns reinforce one another, enhancing the likelihood they will be detected as false positives (*3*). In addition, the time saving afforded by 1D NUS are typically modest. 2D NUS (e.g. the two indirect dimensions of a 3D

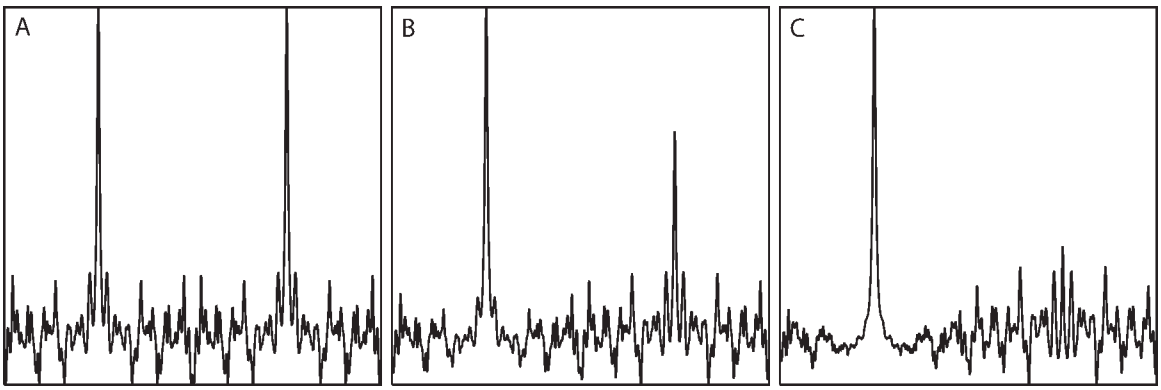

Figure 8 Effective sensitivity of NUS data. Weak peaks in the presence of strong ones can be masked by sampling artifacts associated with the larger peak. Note also the decrease in sampling artifacts about the left peak as the right hand peak decreases in intensity (A–C).

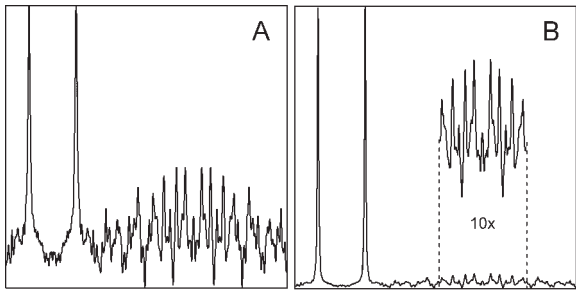

Figure 9 (A) nuDFT vs. (B) MaxEnt reconstruction of the same data. The insert in B shows a 10-fold expansion of the baseline.

experiment) methods, on the other hand, avoid column-wise coherence and the time saving afforded by NUS increases geometrically, i.e. as the product of the time reductions along each dimension. Thus high-dimensional experiments can be rendered practical by multidimensional NUS.

While multidimensional NUS retains many properties of one-dimensional NUS, there are other important differences. Before exploring these differences, we will explore the distinction between on-grid and off-grid NUS.

The Nyquist Grid

We previously discussed that using the DFT the Nyquist condition imposes the constraint that equispaced time points must be sampled in order to avoid aliasing. The interval between the data points is determined by the band-width one wishes to unambiguously observe in the frequency domain (i.e. SW). In two dimensions the same principle applies and one must define SW in each dimension separately. The resulting time points (equispaced in each dimension) form a grid. We refer to this Cartesian grid as the Nyquist grid, which defines the least dense set of time-points required to reconstruct a 2D spectrum free of aliases (see Fig. 11). The Fourier grid is the frequency-domain grid derived from application of the DFT to data sampled on the Nyquist grid.

In 2D, NUS sampling strategies can be described as on-grid when a subset of the Nyquist grid is sampled (similar to 1D NUS), or off-grid, when the sample points fall off the Nyqusit grid. Radial sampling employed by BPR, GFT, and RD methods in general leads to data samples that do not fall on the Nyquist grid. Spectra computed using these methods are usually interpolated in some fashion onto the Fourier grid. Bretthorst has pointed out, however, that in principle it is possible to define a grid for an arbitrary sampling scheme so long as the sample times are specified with finite precision (*29*). The relevant grid is determined by the greatest common divisor (GCD) of the set of sample times, which is usually much smaller than the Nyquist interval.

Regular and Irregular Sampling Schedules

An advantage of radial sampling is that along any projection angle the data is sampled uniformly (Fig. 11), which permits the cross-section to be transformed to the frequency domain using the DFT without introducing sampling artifacts along the reduced dimensionality axis. Sampling artifacts are invariably present in the higher dimensional plane, however, as the sampling is incomplete there (whether computed by PR or MaxEnt, see Fig. 12). In PR these artifacts are manifest as ridges in the back-projected spectrum. The relationship between back projection and NUS has been further demonstrated by use of an on-grid sampling schedule approximating off-grid radial sampling (*17*). The reconstructed spectrum using either approach produces similar artifacts (Fig. 12). This indicates that the ridges produced in PR are due to the sampling scheme, not the reconstruction.

As demonstrated above, regular (e.g. radial) sampling leads to coherent artifacts; it follows that by sampling time points on the Nyquist grid using an irregular scheme such artifacts should de-cohere. Pseudo-random sampling is one way to produce irregular sampling. It has been shown that the coherent artifacts associated with regular sampling schemes can be reduced through the introduction of random "blurring" (*18*). This approach obviates the use of BPR, however, and requires the use of a more general method of spectrum analysis.

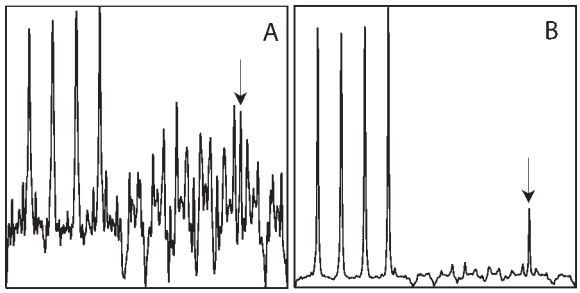

Figure 10 MaxEnt of NUS data. Panel A shows the nuDFT of five synthetic, noiseless signals. Panel B shows the MaxEnt reconstruction of the same data. MaxEnt reconstruction greatly diminishes the sampling artifacts obscuring the smaller peak on the right hand side.

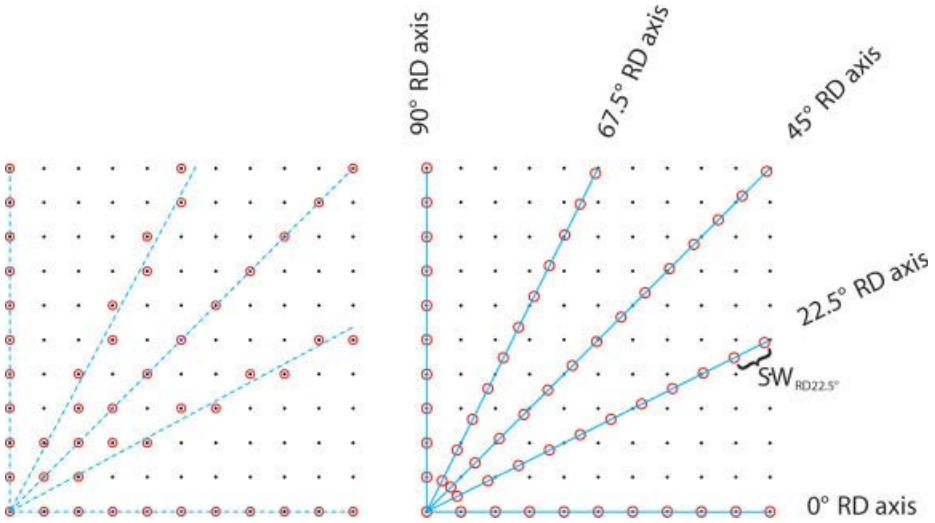

Figure 11 Radial sampling (A) on-grid and (B) off-grid. Dots represent the Nyquist grid, circles represent sampled data points. The solid lines indicate the angle of the radial vector (projection axis). [Color figure can be viewed in the online issue, which is available at www.interscience.wiley.com.]

Finally we show in Fig. 13 that when the data is sampling limited, irregular sampling produces incoherent sampling artifacts that are much lower in intensity than the coherent artifacts produced by regular NUS sampling. Since sensitivity is fundamentally the ability to distinguish true signals from artifacts, higher sensitivity will be obtained using fewer sample points if they are irregularly spaced.

The reduction in sampling that can be achieved using NUS depends on several factors, including the dynamic range, S/N, sparsity, and dimensionality of the signal, as well as the sampling strategy. Figure 14 illustrates that the gains typically increase geometrically with the number of NUS dimensions. It is apparent that for a single NUS dimension there is a dramatic increase in the amplitude of sampling artifacts when the sampled subset represents between 40 and 20% of uniform sampling. For 2D NUS, the dramatic increase occurs between 3 and 2%. The modest increase with increased dimensionality in the number

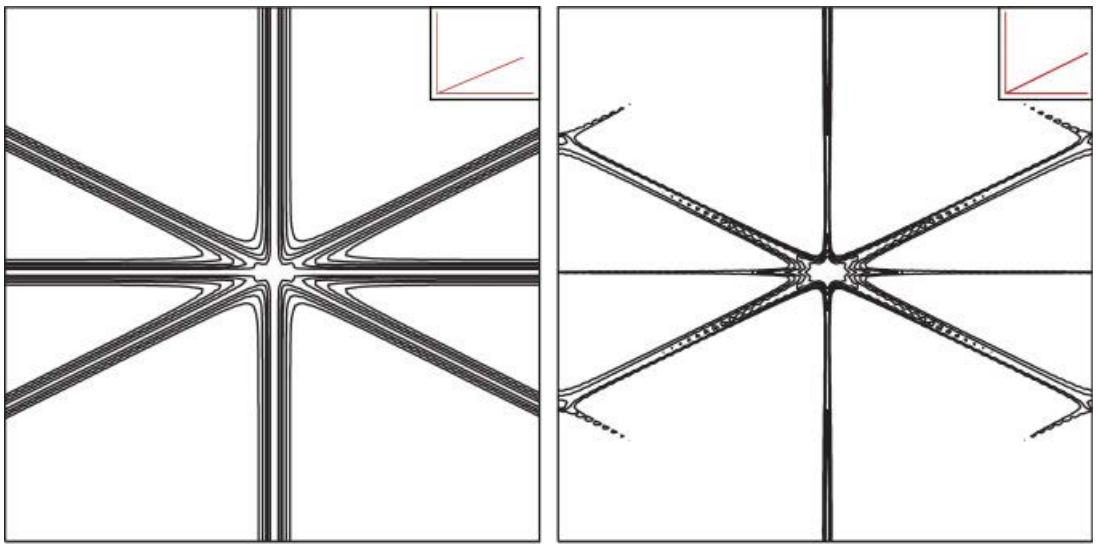

Figure 12 Reconstruction of radially sampled data; off-grid sampled data reconstructed using PR (left); and on grid sampling reconstructed using MaxEnt (right). The insets depict the sampling scheme. [Color figure can be viewed in the online issue, which is available at www.interscience.wiley.com.]

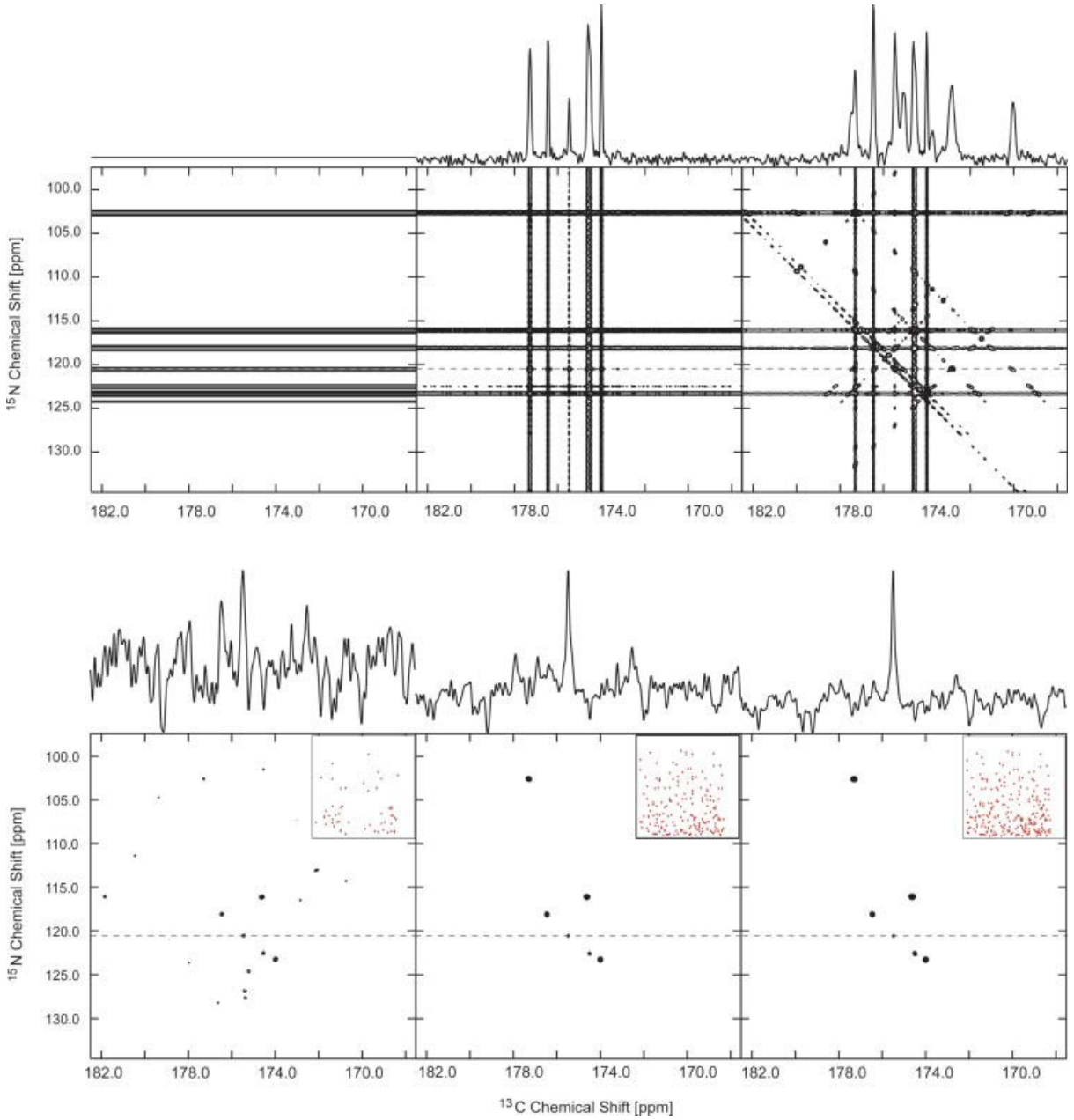

Figure 13 HNCO spectra of ubiquitin. Top panels show the addition of 0°, 90°, and 30° projections of the two jointly sampled indirect dimensions at a proton chemical shift of 8.14 ppm, reconstructed using back projection reconstruction. Each projection contains 52 complex points, thus the total number of complex points sampled, from left to right is 52, 104, and 156. The lower panel shows MaxEnt reconstruction using the same number of complex data points, distributed randomly along the nitrogen dimension (constant time) and with a exponentially decreasing sampling density decay rate corresponding to 15 Hz in the carbon dimension. A 1D trace at the position of the weakest peak present in the spectrum is shown at the top of each spectrum (indicated by a dashed line). The insets depict the sampling scheme. The MaxEnt reconstruction parameters were selected using an automated protocol (*39*, *40*). [Color figure can be viewed in the online issue, which is available at www.interscience.wiley.com.)

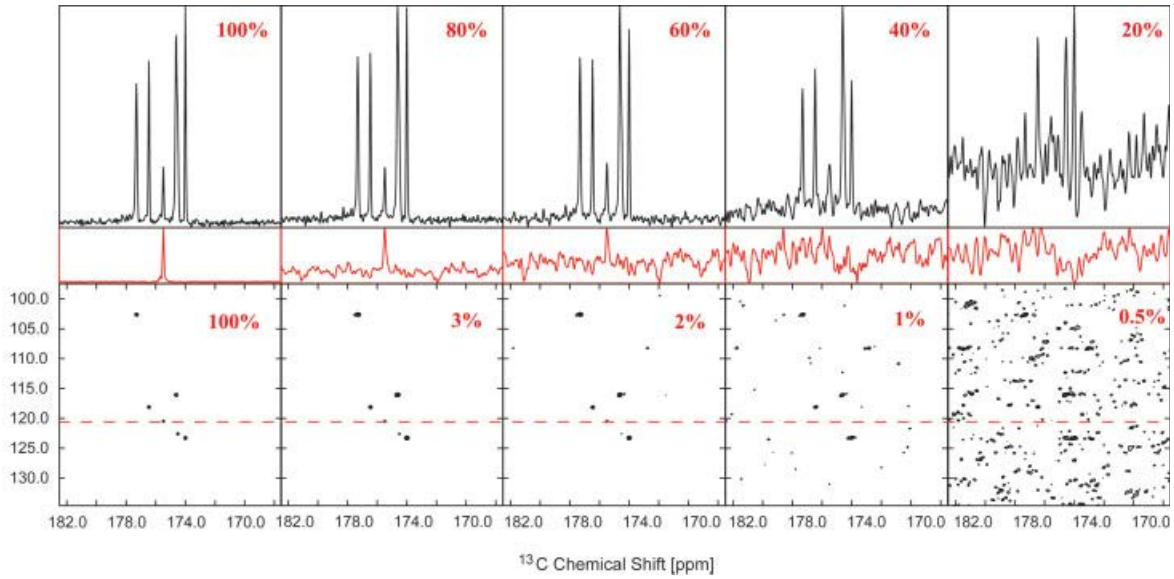

Figure 14 HNCO spectra of ubiquitin. **Top** panels show projections on NUS MaxEnt spectra onto the carbon dimension for the same plane as Fig. 13, using NUS along the carbon indirect dimension and uniform sampling along the other dimensions. The NUS sets were selected using exponential biased random sampling with a sampling density decay rate corresponding to 20 Hz, and retaining 80, 60, 40, and 20% of the samples from the uniform Nyquist grid (100%, shown in the left-most panel). Note the dramatic increase in sampling artifacts between 40 and 20%. The **bottom** panels depict MaxEnt NUS spectra of the same plane, this time using NUS along both the carbon and nitrogen indirect dimensions. The **middle** panels depict one-dimensional traces through the plane at the frequency indicated by a dashed line on the contour plots. The NUS sets were selected using fully random sampling in the (constant time) nitrogen dimension and exponentially biased random sampling with a sampling density decay corresponding to 20 Hz in the carbon dimension. The NUS sets correspond to 3, 2, 1, and 0.5% of the samples from the uniform Nyquist grid (shown in the left-most panel). For 2D NUS, the dramatic increase in sampling artifacts occurs between 3 and 2%. [Color figure can be viewed in the online issue, which is available at www.interscience.wiley.com.]

of samples required to faithfully reconstruct a spectrum, compared to the increase in the number of elements in the Fourier grid is a fairly general property of nonlinear reconstruction methods, including not only MaxEnt reconstruction, but minimum l_1-norm reconstruction, Bayesian, MLM, and MDD methods, as well. These methods tend to perform well when the spectrum is "nearly black," that is there are relatively few nonzero elements in the spectrum (also called sparse support) (*41*). In essence the number of unknowns (the amplitudes and phases of the signal components) do not increase as the dimensionality of the experiment increases. Thus rather dramatic reductions in sampling, compared to the size of the reconstructed spectrum, have been demonstrated for 5–10D experiments (*5, 42, 43*), rendering them feasible in reasonable amounts of acquisition time. In contrast, for multidimensional experiments that are information-rich (large number of unknowns) such as NOESY spectra, much less dramatic reductions in experiment time have been achieved (*44*).

Optimal Sampling

What constitutes an "optimal" sampling schedule depends on the information sought from and constraints imposed by the experiment. We have already seen that the choice of samples exhibits a familiar sensitivity-resolution tradeoff, with sensitivity enhanced by collecting more samples when the time domain signal is strongest (usually at short times) and resolution enhanced by sampling at longer times. Irregular as opposed to regular sampling diminishes sampling artifacts, and selecting samples from an oversampled grid forces some sampling artifacts to high frequencies, out of the band-limited spectral window. Beyond these general observations, how-

ever, critical comparison of different approaches to NUS is hampered by a present lack of consensus on metrics for measuring performance and a lack of common test data. Until such critical comparisons are available, we are limited to offering a few general and practical recommendations for exploiting NUS in multidimensional NMR:

- Do not sample beyond $1.5T_2$*, unless you have very concentrated samples $>$ 1–5 mM; sampling further reduces S/N (*3*, *45*).
- A good compromise between sensitivity and resolution is obtained by matching the sampling density to the signal envelope. Higher sensitivity can be achieved by devoting even more samples to parts of the signal envelope that are strongest. For exponentially decaying signals we find a distribution that decays 2–3 times faster than T_2* works well (*45*).
- Introduce irregularity, either by sampling from a biased random distribution or by random blurring (*18*).
- For experiments with high dynamic range (greater than 20:1), or when you do not know the dynamic range a priori, be conservative. Do not expect to reduce sampling much beyond 1/3rd of the samples on a Nyquist grid of comparable resolution (maximum evolution time) for each NUS time domain, i.e. about an order of magnitude reduction for NUS in two dimensions. However, for particularly sensitive experiments or when signals are sparse much larger reductions in sampling time are feasible (*41*).

CONCLUDING REMARKS

The advantages of NUS can be exploited by several different approaches, but it is clear that NUS introduces ambiguities in the form of sampling artifacts, regardless of the sampling strategy or method of spectral reconstruction. Careful design of the sampling strategy to minimize artifacts is thus essential in order to realize the full potential benefit of NUS. Although NUS artifacts may not be immediately apparent in NUS schemes such as BPR and RD, these artifacts will manifest if the higher-dimensional or "full" spectrum is reconstructed. Approaches such as APSY (*7*) and HIFI (*8*) avoid reconstruction of the full spectrum and attempt to resolve the ambiguities caused by NUS artifacts through logical analysis of peak lists derived from projected cross-sections, rather than from the full spectrum. An advantage to spectral reconstruction, however, is that it is compatible with existing spectral analysis and visualization software tools. A final word of caution: the presence of sampling artifacts and the nonlinearity of methods of spectrum analysis used with NUS data implies that S/N is no longer a reliable indicator of sensitivity (*38*). Proper error analysis to ensure that sampling artifacts and nonlinearity are properly accounted for is paramount.

ACKNOWLEDGMENTS

The authors thank Alan Stern, Mark Maciejewski, David Donoho, and Eriks Kupce for illuminating discussions. This work was supported by grants from the US National Institutes of Health (RR020125, GM47467, GM072000).

REFERENCES

1. Kennedy MA, Montelione GT, Arrowsmith CH, Markley JL. 2002. Role for NMR in structural genomics. J Struct Funct Genomics 2:155–169.
2. Koehl P. 1999. Linear prediction spectral analysis of NMR data. Prog Nucl Magn Reson Spectrosc 34:257–299.
3. Stern AS, Li K, Hoch JC. 2002. Modern spectrum analysis in multidimensional NMR spectroscopy: comparison of linear prediction extrapolation and maximum-entropy reconstruction. J Am Chem Soc 124:1982–1993.
4. Marion D. 2005. Fast acquisition of NMR spectra using Fourier transform of non-equispaced data. J Biomol NMR 32:141–150.
5. Malmodin D, Billeter M. 2005. Multiway decomposition of NMR spectra with coupled evolution periods. J Am Chem Soc 127:13486–13487.
6. Kupče Ē, Freeman R. 2005. Fast multidimensional NMR: radial sampling of evolution space. J Magn Reson 173:317–321.
7. Hiller S, Fiorito F, Wüthrich K. 2005. Automated projection spectroscopy (APSY). Proc Natl Acad Sci USA 102:10876–108881.
8. Eghbalnia HR, Bahrami A, Tonelli M, Hallenga K, Markley JL. 2005. High-resolution iterative frequency identification for NMR as a general strategy for multidimensional data collection. J Am Chem Soc 127:12528–12536.
9. Coggins B, Venters RA, Zhou P. 2005. Filtered back-projection for the reconstruction of a high-resolution (4,2)D CH3-NH NOESY spectrum on a 29kDa protein. J Am Chem Soc 127:11562–11563.
10. Freeman R, Kupče E. 2004. Distant echoes of the accordion: reduced dimensionality, GFT-NMR and projection-reconstruction of multidimensional spectra. Concepts Magn Reson 23:63–75.
11. Kim S, Szyperski T. 2003. GFT NMR, a new approach to rapidly obtain precise high-dimensional NMR spectral information. J Am Chem Soc 125:1385–1393.

12. Ding K, Gronenborn AM. 2002. Novel 2D triple resonance NMR experiments for sequential resonance assignments of proteins. J Magn Reson 156:262–268.
13. Orekhov VY, Ibraghimov IV, Billeter M. 2001. MUNIN: a new approach to multi-dimensional NMR spectra interpretation. J Biomol NMR 20:49–60.
14. Chylla RA, Markley JL. 1995. Theory and application of the maximum likelihood principle to NMR parameter estimation of multidimensional NMR data. J Biomol NMR 5:245–258.
15. Coggins BE, Zhou P. 2007. Sampling of the NMR time domain along concentric rings. J Magn Reson 184:207–221.
16. Kazimierczuk K, Kozminski W, Zhukov I. 2006. Two-dimensional Fourier transform of arbitrarily sampled NMR data sets. J Magn Reson 179:323–328.
17. Mobli M, Stern AS, Hoch JC. 2006. Spectral reconstruction methods in fast NMR: reduced dimensionality, random sampling and maximum entropy. J Magn Reson 182:96–105.
18. Hoch JC, Maciejewski MW, Filipovic B. 2008. Randomization improves sparse sampling in multidimensional NMR. J Magn Reson 193:317–320.
19. Ernst RR, Anderson WA. 1966. Application of fourier transform spectroscopy to magnetic resonance. Rev. Sci. Instru. 37:93.
20. Ernst RR, Bodenhausen G, Wokaun A. 1987. Principles of Nuclear Magnetic Resonance in One and Two Dimensions. Oxford: Oxford University Press.
21. Hoch JC, Stern AS. 1996. NMR Data Processing. New York: Wiley-Liss.
22. Simorre J-P, Marion D. 1990. Acquisition schemes and quadrature artifacts in phase-sensitive two-dimensional NMR. J Magn Reson 89:191–197.
23. Rovnyak D, Frueh DP, Sastry M, Sun ZJ, Stern AS, Hoch JC, et al. 2004. Accelerated acquisition of high resolution triple-resonance spectra using non-uniform sampling and maximum entropy. J Magn Reson 170:15–21.
24. Szyperski T, Yeh DC, Sukumaran DK, Moseley HNB, Montelione GT. 2002. Reduced-dimensionality NMR spectroscopy for high-throughput protein resonance assignment. Proc Natl Acad Sci USA 99:8009–8014.
25. Mandelshtam VA, Taylor HS, Shaka AJ. 1998. Application of the filter diagonalization method to one- and two-dimensional NMR spectra. J Magn Reson 133:304–312.
26. Barna JCJ, Laue ED, Mayger MR, Skilling J, Worrall SJP. 1987. Exponential sampling: an alternative method for sampling in two-dimensional NMR experiments. J Magn Reson 73:69–77.
27. Bodenhausen G, Ernst RR. 1982. Direct determination of rate constants of slow dynamic processes by two-dimensional "accordion" spectroscopy in nuclear magnetic resonance. J Am Chem Soc 104:1304–1309.
28. Kupče Ē, Freeman R. 2004. Projection-reconstruction technique for speeding up multidimensional NMR spectroscopy. J Am Chem Soc 126:6429–6440.
29. Bretthorst GL. 2001. Nonuniform sampling: Bandwidth and aliasing. In: Rychert R, Erickson G, Smith CR, eds. Maximum Entropy and Bayesian Methods in Science and Engineering. vol 567 of AIP Conf. Proc. Amer. Inst. Phys., Melville, NY, pp 1–28.
30. Schmieder P, Stern AS, Wagner G, Hoch JC. 1997. Quantification of maximum entropy spectrum reconstructions. J Magn Reson 125:332–339.
31. Hyberts SG, Heffron GJ, Tarragona NG, Solanky K, Edmonds KA, Luithardt H, et al. 2007. Ultrahigh-resolution 1H-13C HSQC spectra of metabolite mixtures using nonlinear sampling and forward maximum entropy reconstruction. J Am Chem Soc 129:5108–5116.
32. Stern AS, Donoho DL, Hoch JC. 2007. NMR data processing using iterative thresholding and minimum l1-norm reconstruction. J Magn Reson 188:295–300.
33. Gull SF, Daniell GJ. 1978. Image reconstruction from incomplete and noisy data. Nature 272:686–690.
34. Brigham EO. 1988. The Fast Fourier Transform: An Introduction to Its Theory and Application. Englewood Cliffs, NJ: Prentice Hall.
35. Kazimierczuk K, Zawadzka A, Kozminski W, Zhukov I. 2007. Lineshapes and artifacts in multidimensional Fourier transform of arbitrary sampled NMR data sets. J Magn Reson 188:344–356.
36. Hoch JC, Stern AS. 2002. Maximum entropy reconstruction, spectrum analysis and deconvolution in multidimensional nuclear magnetic resonance. Methods Enzymol 338:159–178.
37. Kubat JA, Chou JJ, Rovnyak D. 2007. Nonuniform sampling and maximum entropy reconstruction applied to the accurate measurement of residual dipolar couplings. J Magn Reson 186:201–211.
38. Donoho DL, Johnstone IM, Stern AS, Hoch JC. 1990. Does the maximum entropy method improve sensitivity? Proc Natl Acad Sci 87:5066–5068.
39. Mobli M, Maciejewski MW, Gryk MR, Hoch JC. 2007. An automated tool for maximum entropy reconstruction of biomolecular NMR spectra. Nat Methods 4:467–468.
40. Mobli M, Maciejewski M, Gryk M, Hoch J. 2007. Automatic maximum entropy spectral reconstruction in NMR. J Biomol NMR 39:133–139.
41. Donoho DL, Johnstone IM, Hoch JC, Stern AS. 1992. Maximum entropy and the nearly black object. J R Stat Soc Ser B (Methodological) 54:41–81.
42. Kupce E, Freeman R. 2006. Hyperdimensional NMR spectroscopy. J Am Chem Soc 128:6020–6021.
43. Hiller S, Wasmer C, Wider G, Wuthrich K. 2007. Sequence-specific resonance assignment of soluble nonglobular proteins by 7D APSY-NMR spectroscopy. J Am Chem Soc 129:10823–10828.
44. Luan T, Jaravine V, Yee A, Arrowsmith C, Orekhov V. 2005. Optimization of resolution and sensitivity of 4D NOESY using multi-dimensional decomposition. J Biomol NMR 33:1–14.
45. Rovnyak D, Hoch JC, Stern AS, Wagner G. 2004. Resolution and sensitivity of high field nuclear magnetic resonance spectroscopy. J Biomol NMR 30:1–10.